Phase transition and electronic structure evolution of MoTe2 induced by W substitution

Santos, E. J. G. (2018). Phase transition and electronic structure evolution of MoTe2 induced by W substitution. *Physical Review B*, *98*, 144114-144120. https://doi.org/10.1103/PhysRevB.98.144114

Published in:
Physical Review B

Document Version:
Peer reviewed version

Queen's University Belfast - Research Portal:
Link to publication record in Queen's University Belfast Research Portal

Publisher rights
© 2018 American Physical Society. This work is made available online in accordance with the publisher's policies. Please refer to any applicable terms of use of the publisher.

General rights
Copyright for the publications made accessible via the Queen's University Belfast Research Portal is retained by the author(s) and / or other copyright owners and it is a condition of accessing these publications that users recognise and abide by the legal requirements associated with these rights.

Take down policy
The Research Portal is Queen's institutional repository that provides access to Queen's research output. Every effort has been made to ensure that content in the Research Portal does not infringe any person's rights, or applicable UK laws. If you discover content in the Research Portal that you believe breaches copyright or violates any law, please contact openaccess@qub.ac.uk.

Download date:04. May. 2023

Phase transition and electron structure evolution of $MoTe_2$ induced by W substitution

Wencan Jin,[1,*] Theanne Schiros,[2] Yi Lin,[1] Junzhang Ma,[3] Rui Lou,[4] Zhongwei Dai,[5] Jiexiang Yu,[5] Daniel Rhodes,[6] Jerzy T. Sadowski,[7] Xiao Tong,[7] Tian Qian,[3] Jerry I. Dadap,[1] Shancai Wang,[4] Jiadong Zang,[5] Karsten Pohl,[5] Hong Ding,[3] James Hone,[1] Luis Balicas,[6] Abhay N. Pasupathy,[1,†] and Richard M. Osgood, Jr[1,‡]

[1] *Columbia University, New York, New York 10027, USA*
[2] *Fashion Institute of Technology, New York, New York 10001, USA*
[3] *Beijing National Laboratory for Condensed Matter Physics, and Institute of Physics, Chinese Academy of Sciences, Beijing 100190, China*
[4] *Department of Physics, Renmin University of China, Beijing 100872, China*
[5] *University of New Hampshire, Durham, NH 03824, USA*
[6] *Florida State University, Tallahassee, Florida 32306, USA*
[7] *Center for Functional Nanomaterials, Brookhaven National Laboratory, Upton, New York 11973, USA*

The transition metal dichalcogenide compounds $MoTe_2$ and WTe_2 are polymorphic with both semiconducting and metallic phases. The thermodynamically stable phase of WTe_2 at room temperature is monoclinic and metallic, and displays a wide range of interesting phenomena including type-II Weyl fermions, titanic magnetoresistance and superconductivity in the bulk, and quantum spin Hall insulator behavior in the monolayer. On the other hand, the stable phase of $MoTe_2$ at room temperature is a trigonal prismatic semiconductor that has a direct gap in the monolayer with strong spin-orbit coupling. The alloy series $Mo_{1-x}W_xTe_2$ thus offers the possibility of tuning the structural and consequently electronic phases via tuning of the composition. Here, we report comprehensive studies of the electronic structure of $Mo_{1-x}W_xTe_2$ alloys using angle-resolved photoemission spectroscopy and first principle calculations as a function of composition. We find a sharp boundary at room temperature between the monoclinic and trigonal prismatic phases at $x = 0.10$ from structural characterization. We also show that by compositional tuning it is possible to control the band inversion in this series of compounds, with important consequences for the topological surface states.

I. INTRODUCTION

Transition metal dichalcogenides (TMDCs, MX_2, M=Mo, W; X=Se, Te) are polymorphic with different crystal structures, including trigonal prismatic $2H$ phase (Fig. 1(a)), monoclinic $1T'$ phase, and orthorhombic T_d phase (Fig. 1(d)). These phases provide an important platform for exploring exotic physics and novel device applications. The semiconducting $2H$-phase TMDCs in monolayer form consists of a layer of hexagonally arranged transition metal atoms sandwiched between two layers of chalcogen atoms. In monolayer *2H*-TMDCs, the sizeable direct band gap [1–3] and valley degree of freedom [4–6] make this phase remarkably appealing for electronics [7], and spin- and valley-tronics devices [8, 9]. Recently, the metallic $1T'$ and T_d phase have attracted interest due to the presence of band inversion in these phases, making them important candidates for realizing novel topological quantum phenomena. The semimetallic $1T'$ phase exhibits a distorted octahedral structure with an inclined stacking angle of $\sim 93.9°$, which retains a centrosymmetric $P2_1/m$ space group. In contrast, in the orthorhombic T_d phase, the stacking angle is exactly 90°, which breaks inversion symmetry (space group $Pmn2_1$) [10]. The T_d phase displays a number of unique electronic properties in both the bulk and monolayer forms. Bulk crystals of both T_d-WTe_2 [11, 12] and T_d-$MoTe_2$ [13] display a large, non-saturating magnetoresistance, possibly due to electron-hole compensation. Bulk T_d-WTe_2 [14], T_d-$MoTe_2$ [15, 16] as well as some of their alloys [17] are also known to be type-II Weyl fermions. These type-II Weyl fermions are characterized by touching points between electron- and hole-pocket with strongly tilted Weyl cones [14] in the bulk, and Fermi-arc states on the surface. A number of angle-resolved photoemission spectroscopy (ARPES) studies of the electronic structure of T_d-WTe_2 [18–20], $MoTe_2$ [21–24] and $Mo_xW_{1-x}Te_2$ on the W rich side [25, 26] have found evidence for these features. Finally, in monolayer form, the T_d-TMDCs are two-dimensional topological insulators that display the quantum spin Hall effect [13, 27].

The rich electronic phenomenology associated with the semiconducting and metallic phases of these compounds has spurred intense interest in achieving precise control of transitions between these phases. Such phase engineering of TMDCs has recently been attempted using a variety of tuning parameters such as temperature, strain, chemical doping and electrostatic doping [13, 28–32]. Achieving reversible control of the phase transition is important for on-demand topological properties as well as for the development of technological applications such as phase-change memory devices [33, 34]. One of

* Current address: University of Michigan, Ann Arbor, MI 48109, USA
† apn2108@columbia.edu
‡ osgood@columbia.edu

the chief difficulties in achieving this reversible control in the parent compounds $MoTe_2$ and WTe_2 is that they are fairly stable at room temperature. In this context, alloying has been shown by some of us to play an important role in structural phase control (reference previous work). Briefly, at room temperature, the thermodynamically stable phase of $MoTe_2$ is the semiconducting $2H$ polymorph. In contrast, the stable phase of WTe_2 is the semimetallic T_d polymorph. By using chemical alloying to produce the series $Mo_{1-x}W_xTe_2$, we showed the existence of a phase transition at around x=0.08. We expect that as we approach the critical doping that the alloys become sensitive to dynamical tuning parameters such as strain and electrostatic doping, opening up new possibilities for structural control. As we approach this critical doping, we must understand the electronic structure of the alloys on either side of the phase transition in details. In this work, we achieve this by performing synchrotron-based ARPES measurements of $Mo_{1-x}W_xTe_2$ as a function of W concentration, supported by structural characterization and density functional theory. The major findings of our study show that (i) the phase transition from $2H$ to T_d appears on the Mo-rich side (critical W concentration $x_c \sim 0.10$) of the alloy composition point, in contrast to the previously predicted value of 0.33 [35]; (ii) W doping results in a downward shift of conduction band minimum, thus enhancing the band inversion; and (iii) demonstration via density functional theory calculation that interlayer coupling in this material is weaker than in widely studied TMDCs like MoS_2.

These predictions for type-II Weyl fermions have triggered a series of angle-resolved photoemission spectroscopy (ARPES) studies of the electronic structure of T_d-WTe_2 [18–20], $MoTe_2$ [21–24] and $Mo_xW_{1-x}Te_2$ on the W rich side [25, 26]. These measurements have shown that the size of the Fermi arc in WTe_2 is extremely small due to the small separation of the Weyl points, while the Fermi arc of $MoTe_2$ is more extended in momentum space, indicating the topological strength of the latter is more robust. Therefore, $Mo_{1-x}W_xTe_2$ alloy on the Mo rich side, in comparison with the W-rich counterpart, is more appealing for investigation of the electronic structure evolution and tunable topological strength. In addition, $MoTe_2$ exists 2H, $1T'$ and T_d phases, while WTe_2 has commonly been observed in the T_d structure. It is technically more efficient to induce a phase transition in $MoTe_2$ by W doping, instead of doping Mo to WTe_2. To this end, Mo-rich $Mo_{1-x}W_xTe_2$ alloys makes an ideal playground for exploring the structural phase transition and electronic structure evolution, and thus there is a pressing need for a comprehensive experimental investigation.

In this work, we report electronic structure evolution of $Mo_{1-x}W_xTe_2$ as a function of W concentration using synchrotron-based ARPES and in concert with density functional theory calculations. The major findings of our study show that (i) the phase transition from $2H$ to T_d appears on the Mo-rich side (critical W concentration $x_c \sim 0.10$) of the alloy composition point, in contrast to the previously predicted value of 0.33 [35]; (ii). W doping results in a downwards shift of conduction band minimum, thus enhancing the band inversion; and (iii) demonstration via density functional theory calculation that interlayer coupling in this material is weaker than in widely studied TMDCs like MoS_2.

II. RESULTS AND DISCUSSION

The synthesis method for our crystals has been detailed in Ref.[36]. Prior to our ARPES measurements, the composition of the alloys was first determined with x-ray photoemission spectroscopy (XPS) as described in the Methods section. The crystalline structure of $Mo_{1-x}W_xTe_2$ alloys was then investigated using selected-area low energy electron diffraction (μ-LEED) at room temperature. The well-defined hexagonal μ-LEED pattern (see Fig. 1(b)) acquired from $x = 0.08$ alloy, demonstrates that the alloys with $x < x_c$ crystallize in the 2H-phase. In comparison, the rectangular μ-LEED pattern (Figs. 1 (e)) for a crystal of composition of $x = 0.16$ shows that moderate W substitution ($x > x_c$) has stabilized the T_d-phase at room temperature. Note that multiple locations were surveyed across the sample surface, and no phase coexistence was observed. In addition, to examine any major changes in crystal structure within surface layers, we determined the surface structure of these $Mo_{1-x}W_xTe_2$ alloys using dynamical LEED calculations[37–39]. The measured LEED-I-V (blue solid curve) for the (00) diffraction beam and calculated I-V (black dashed curve) are shown in Fig. 1 (c) and (f). The optimized surface structure for $2H$- and T_d phase were obtained by fitting the calculated I-V curves to the measured ones, and the results indicate that surface structure while distinct from that in the bulk is not significantly different enough to change the electronic structure.

ARPES measurements were then used to investigate the electronic structure of $Mo_{1-x}W_xTe_2$ alloys; to sharpen the spectra the measurements were made at low temperature, typically 50 K. Figure. 2 (a) shows the ARPES bandmap of $2H$-$Mo_{0.94}W_{0.06}Te_2$ alloy along the $\bar{K}$-$\bar{\Gamma}$-$\bar{K}$ high-symmetry direction of the surface Brillouin zone (see inset). The corresponding integrated spectrum (Fig. 2 (b)) shows that the main band features are derived from the Mo d_{z^2} and Te p_z orbitals. The conduction bands were not observed up to 1 eV above valence band maximum (VBM), confirming $2H$-phase is semiconducting with a gap size > 1 eV. The band features are further displayed as corresponding energy distribution curves (EDCs) plots in Fig. 2 (c). A

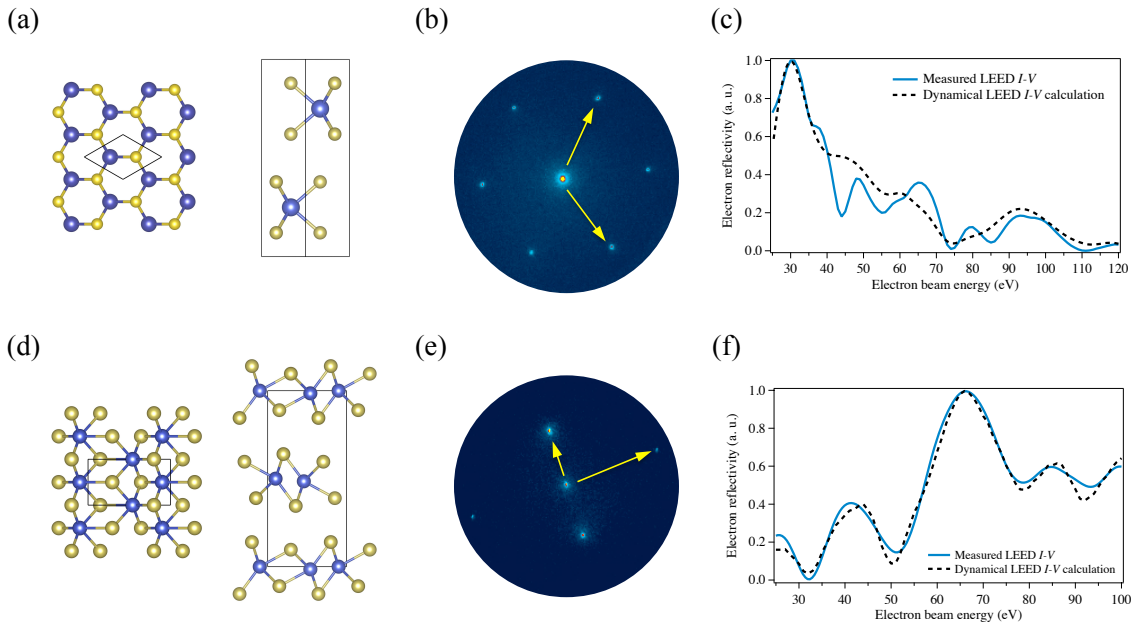

FIG. 1. **Crystalline structure of 2*H*- and T_d- $Mo_{1-x}W_xTe_2$ crystals**. (a) Schematic of $2H$-phase atomic structure in top view (left) and sideview (right), (b) LEED pattern, and (c) μ-LEED I-V curve for $2H$-$Mo_{0.92}W_{0.08}Te_2$.(d) Schematic of T_d-phase atomic structure in topview (left) and sideview (right), (e) LEED pattern, and (f) μ-LEED I-V curve for T_d-$Mo_{0.84}W_{0.16}Te_2$. Blue spheres: Mo/W atoms; yellow spheres: Te atoms.

parabolic fit of the topmost valence band yields a hole effective mass at $\bar{\Gamma}$ of $3.77m_0$ (where m_0 is the electron mass), which is even larger than that of monolayer MoS_2 ($\sim 2.4m_0$). As revealed, the thickness-dependent electronic structure of MoS_2 [2], the topmost valence band at $\bar{\Gamma}$ decreases in energy with decreasing interlayer coupling strength, which leads to increasing hole effective mass. The remarkably flat topmost valence band implies rather weak interlayer coupling in $2H$-$Mo_{0.94}W_{0.06}Te_2$ alloy.

In contrast to the semiconducting $2H$ phase, the ARPES bandmap (Fig. 2 (e)) of the T_d-phase (x = 0.2) along $\bar{Y}$-$\bar{\Gamma}$-$\bar{Y}$ (Fig. 2 (d)) high symmetry direction shows a metallic nature, in which a hole band (yellow arrow, α) and electron pocket (white arrow, β) both cross the Fermi level. In addition, the surface state (red, SS) protrudes the electron pocket and almost overlaps with the hole band, which indicates that it is derived from a type-B surface [19]. These band features are further displayed in the EDCs plot (Fig. 2 (f)). Figure 2 (g) shows the stack of constant-energy maps. In particular, a palmier-shaped hole pocket and an almond-shaped electron pocket are observed in the Fermi surface ($E = E_F$) map. The sizes of hole and electron pockets increase and decrease with increasing binding energy, respectively. We have comprehensively measured the electronic structure evolution of the T_d phase as a function of W concentrations. A side-by-side comparison of the electronic structure is made between $x = 0.16$, $x = 0.20$, and $x = 0.27$. As shown in the ARPES bandmaps and corresponding second derivative plots in Fig. 3(a)-(c), the overlap in energy between valence and conduction band decreases with increasing W concentration. Such overlap is characterized by the energy postion of the conduction band minimum (CBM), as shown in the EDC plots (Fig. 3(d)). The CBM of $x = 0.16$ is located at ~ 50 meV, which is comparable with that of pure T_d-$MoTe_2$ (60 meV) [21]. As the W concentration increases, the CBM shifts towards the Fermi level, and in the $x = 0.27$ alloy, the overlap is significantly suppressed, given the large content of Mo relative to W. While we do not directly visualize the Weyl crossings in this data set, it is clear that the change in the band inversion also tunes the separation between Weyl points and consequently the surface state band structure.

To further investigate the band inversion observed here, we use density functional theory calculations to study the evolution of the electronic structure with alloying. Our previous photon energy-dependent ARPES studies [36] and theoretical calculations [40] have revealed that the dispersion along k_z direction shows two-dimensional character. Here, we employ a model at the 2D limit by considering only one unit cell (1UC) thickness of the T_d structure (see Fig. 1(d)). Figure 4(a) shows the calculated hole band and electron pocket as a function of W concentration. As W concentration increases, the hole band slightly sinks down while the electron pocket rapidly shifts upwards. Our 1UC model

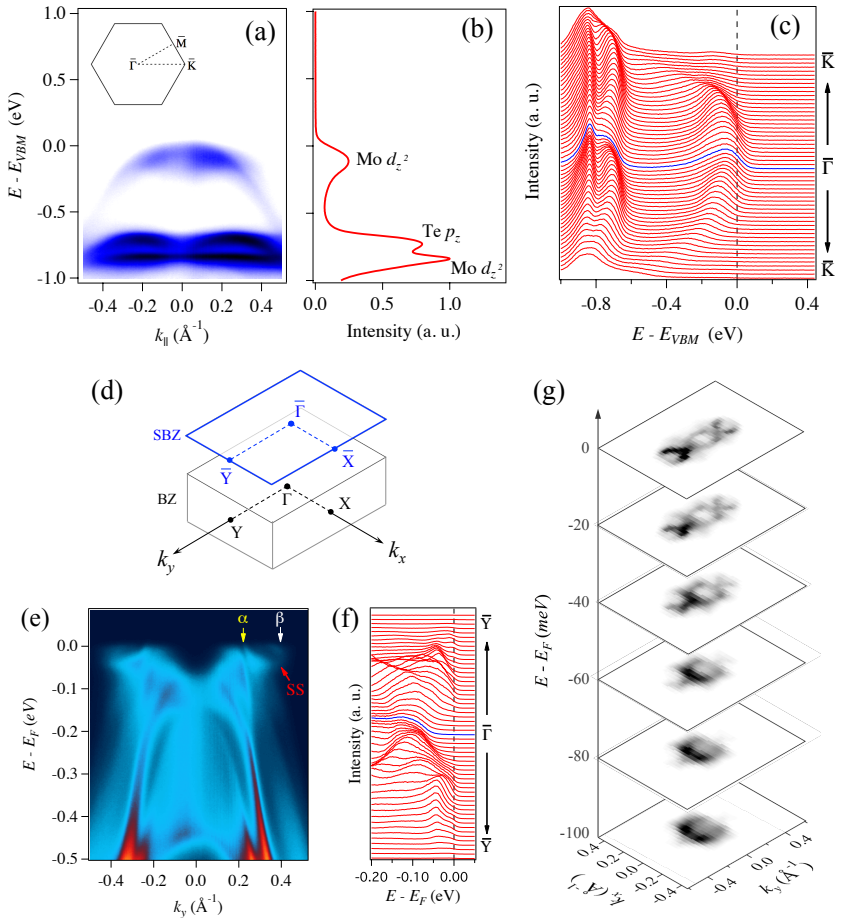

FIG. 2. **Electron structure of $Mo_{1-x}W_xTe_2$ alloys across critical W concentration.** Electronic structure of 2H-$Mo_{0.94}W_{0.06}Te_2$ alloy (a) ARPES bandmap along $\bar{K}$-$\bar{\Gamma}$-$\bar{K}$ high symmetry direction, inset shows the surface Brillouin zone (b) Integrated spectrum and (c) EDCs plot of ARPES bandmap shown in (a). Electronic structure of T_d-$Mo_{0.80}W_{0.20}Te_2$ alloy (d) the bulk Brillouin zone (BZ) and projected (001) surface Brillouin zone (SBZ), (e) ARPES bandmap ($h\nu$ = 24 eV) along $\bar{Y}$-$\bar{\Gamma}$-$\bar{Y}$ high symmetry direction, (e) EDCs plot of band features near Fermi level (E_F), and (g) stack of constant energy maps.

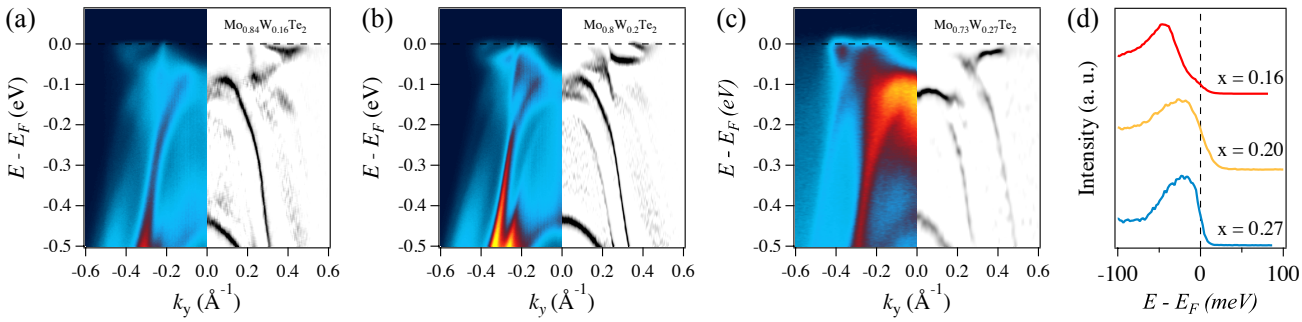

FIG. 3. **Electronic structure evolution for different T_d-$Mo_{1-x}W_xTe_2$ alloys with W concentrations.** ARPES bandmap (left) and corresponding second-derivative intensity plot (right) of T_d-$Mo_{1-x}W_xTe_2$ alloys along $\bar{Y}$-$\bar{\Gamma}$-$\bar{Y}$ high symmetry direction with (a) x = 0.16, (b) x = 0.20, and (c) x = 0.27. (d) Corresponding EDCs across conduction band minimum.

capture the measured band inversion evolution very well. This result further confirms the 2D character of the electronic ~~strucrure.~~ First principle calculations can also give us insight into the structural stability of the $2H$ and T_d phases as a function of alloying. To clarify this question, we first investigated both the $2H$ and T_d phase of the bulk and monolayer structures of pure $MoTe_2$ and WTe_2. To directly compare the total energy between $2H$ and T_d phase with different W concentration, we employ an expanded supercell containing 12(24) Mo/W atoms for 1UC (bulk) cases. This supercell can be regarded as a 3×2 supercell of the primitive cell for T_d phase. The energy difference per Mo/W atom between $2H$ and T_d are shown in Fig. 4(b). The energy difference as a function of doping value x is nearly a linear relationship, which leads to a phase transition point at $x = 0.25$ for bulk and $x = 0.13$ for 1UC case. Here, the phase transition point predicted by bulk model is close to that of previous study, while the 1UC model more accurately capture the measured critical doping value ($x_c \sim 0.10$), which further confirms that $Mo_{1-x}W_xTe_2$ crystal is close to a 2D system rather than a vdW system.

III. CONCLUSION

In conclusion, we investigate the structural phase transition and electronic structure evolution of $Mo_{1-x}W_xTe_2$ alloys using ARPES and DFT calculations. Our results show that a critical W concentration of $x \sim 10\%$ trigger a phase transition from 2H to T_d phase, and in the T_d phase, topological strength is significantly suppressed by increasing W doping. The phase transition point and electronic structure evolution is captured well by the DFT calculations using a 1UC model, indicating the 2D character of this material due to weak interlayer coupling.

IV. METHODS

X-ray photoemission spectroscopy Stoichiometry of alloys were determined by x-ray photoelectron spectroscopy (XPS) at the RHK Technology UHV 7500 facility at Center for Functional Nanomaterials at Brookhaven National Laboratory. The samples were cleaved *in-situ* with a pressure $< 10^{-9} Torr$. The XPS experiments were conducted at room temperature using Mg K_α line with an energy resolution of 0.9 eV.

Angle-resolved photoemission spectroscopy. ARPES measurements were performed at the Dreamline beamline of the Shanghai Synchrotron Radiation Facility (SSRF) with a Scienta D80 analyzer. The samples were measured at 40 K with a base pressure $< 5 \times 10^{-11}$ Torr. The ARPES data were collected within 12 hours after cleavage, during which time no signature of surface degradation was observed. The energy and angular resolutions were set to 15 meV and 0.2°, respectively. (Need input from Theanne about Stanford Synchrotron Radiation Lightsource.)

Low energy electron microscopy. μ-LEED measurements were performed at the Center for Functional Nanomaterials, Brookhaven National Laboratory using an ELMITEC AC-LEEM system. In this system, the sample was cleaved *in situ* at room temperature. The spatial resolution is <3 nm in the LEEM mode. The electron-beam spot size in the μ-LEED mode is 5 µm in diameter.

First-principles electronic structure calculation. Density functional theory calculation was carried out using a VASP package [41] with a projector augmented plane-wave potential [42]. The exchange-correlation energy was described by the generalized gradient approximation in Perdew, Burke, and Ernzerhof (PBE) form [43]. The Brillouin zone of the orthogonal unit cell of T_d-$Mo_{1-x}W_xTe_2$ were sampled by a 7×12×3 k-point mesh. The energy cutoff was set to 440eV. Van der Waals interactions were incorporated within the Tkatchenko-Scheffler method [44]. Spin-orbit coupling was also included for structural optimization. All structures were optimized until the atomic force on each atom with both Hellmann-Feynman and van der Waals terms were taken into acount, is less than 1meV/Å. For one unit cell case, a vacuum layer of 15 Å is used to build 2D slabs.

Dynamical LEED Calculation. The codes from Adams *et al.* [45], which were developed from the programs of Pendry [46] and Van Hove and Tong [47], were used in the dynamical LEED calculations. The lattice constants of WTe_2 are a = 6.282 Å, b = 3.496 Å, c = 14.07 Å [48]. The lattice constants of $MoTe_2$ are a = 6.335 Å, b = 3.477 Å, c = 13.883 Å [15]. As the lattice contant difference between $MoTe_2$ and WTe_2 is less than 1.5%, we use the weighed average as the lattice contants of $Mo_{1-x}W_xTe_2$ alloys. The Debye temperature for $Mo_{1-x}W_xTe_2$ was set as 210K. The inner potential of $Mo_{1-x}W_xTe_2$ is set as 10.1 eV. 12 (L = 11) phase shifts are used in the calculation.

V. ACKNOWLEDGEMENTS

The LEEM/LEED research was carried out in part at the Center for Functional Nanomaterials, Brookhaven National Laboratory, was supported by the U.S. Department of Energy, Office of Basic Energy Sciences, under Contract No. DE-SC0012704. The work of R.M.O., J.D., W.J. and Y.L. was financially supported by the U.S. Department of Energy under Contract No. DE-FG 02-04-ER-46157. In addition, Z.W.D., and K.P. were supported by NSF DMR 1006863. R.L. and S.C.W. were supported

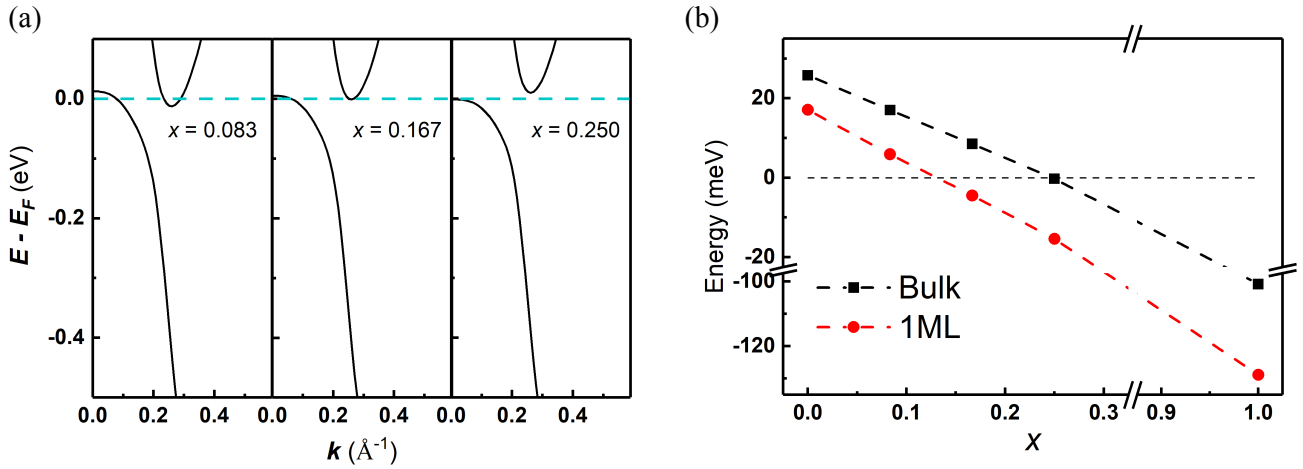

FIG. 4. (a) DFT calculated hole band and electron pocket with various W concentrations. (b) The calculated energy difference between $2H$ and T_d phase as a function of doping value x of $Mo_{1-x}W_xTe_2$ for both bulk and 1UC.

by the National Natural Science Foundation of China (No. 11274381). J.Z.M., T.Q., and H.D. were supported by the Ministry of Science and Technology of China (No. 2015CB921300, No. 2013CB921700), the National Natural Science Foundation of China (No. 11474340, No. 11234014), and the Chinese Academy of Sciences (No. XDB07000000). (Need funding acknowledgement from Elton, Theanne and Prof. Pasupathy.)

[1] K. F. Mak, C. Lee, J. Hone, J. Shan, and T. F. Heinz, Physical Review Letters **105**, 136805 (2010).
[2] W. Jin, P.-C. Yeh, N. Zaki, D. Zhang, J. T. Sadowski, A. Al-Mahboob, A. M. van Der Zande, D. A. Chenet, J. I. Dadap, I. P. Herman, *et al.*, Physical Review Letters **111**, 106801 (2013).
[3] Y. Zhang, T.-R. Chang, B. Zhou, Y.-T. Cui, H. Yan, Z. Liu, F. Schmitt, J. Lee, R. Moore, Y. Chen, *et al.*, Nature Nanotechnology **9**, 111 (2014).
[4] D. Xiao, G.-B. Liu, W. Feng, X. Xu, and W. Yao, Physical Review Letters **108**, 196802 (2012).
[5] K. F. Mak, K. He, J. Shan, and T. F. Heinz, Nature Nanotechnology **7**, 494 (2012).
[6] T. Cao, G. Wang, W. Han, H. Ye, C. Zhu, J. Shi, Q. Niu, P. Tan, E. Wang, B. Liu, *et al.*, Nature Communications **3**, 887 (2012).
[7] Q. H. Wang, K. Kalantar-Zadeh, A. Kis, J. N. Coleman, and M. S. Strano, Nature Nanotechnology **7**, 699 (2012).
[8] K. F. Mak, K. L. McGill, J. Park, and P. L. McEuen, Science **344**, 1489 (2014).
[9] H. Zeng, J. Dai, W. Yao, D. Xiao, and X. Cui, Nature Nanotechnology **7**, 490 (2012).
[10] K. Zhang, C. Bao, Q. Gu, X. Ren, H. Zhang, K. Deng, Y. Wu, Y. Li, J. Feng, and S. Zhou, Nature Communications **7** (2016).
[11] M. N. Ali, J. Xiong, S. Flynn, J. Tao, Q. D. Gibson, L. M. Schoop, T. Liang, N. Haldolaarachchige, M. Hirschberger, N. Ong, *et al.*, Nature **514**, 205 (2014).
[12] L. Thoutam, Y. Wang, Z. Xiao, S. Das, A. Luican-Mayer, R. Divan, G. Crabtree, and W. Kwok, Physical Review Letters **115**, 046602 (2015).
[13] D. H. Keum, S. Cho, J. H. Kim, D.-H. Choe, H.-J. Sung, M. Kan, H. Kang, J.-Y. Hwang, S. W. Kim, H. Yang, *et al.*, Nature Physics **11**, 482 (2015).
[14] A. A. Soluyanov, D. Gresch, Z. Wang, Q. Wu, M. Troyer, X. Dai, and B. A. Bernevig, Nature **527**, 495 (2015).
[15] Y. Sun, S.-C. Wu, M. N. Ali, C. Felser, and B. Yan, Physical Review B **92**, 161107 (2015).
[16] Z. Wang, D. Gresch, A. A. Soluyanov, W. Xie, S. Kushwaha, X. Dai, M. Troyer, R. J. Cava, and B. A. Bernevig, Physical Review Letters **117**, 056805 (2016).
[17] T.-R. Chang, S.-Y. Xu, G. Chang, C.-C. Lee, S.-M. Huang, B. Wang, G. Bian, H. Zheng, D. S. Sanchez, I. Belopolski, *et al.*, Nature communications **7**, 10639 (2016).
[18] J. Sánchez-Barriga, M. Vergniory, D. Evtushinsky, I. Aguilera, A. Varykhalov, S. Blügel, and O. Rader, Physical Review B **94**, 161401 (2016).
[19] F. Y. Bruno, A. Tamai, Q. Wu, I. Cucchi, C. Barreteau, A. De La Torre, S. M. Walker, S. Riccò, Z. Wang, T. Kim, *et al.*, Physical Review B **94**, 121112 (2016).
[20] C. Wang, Y. Zhang, J. Huang, S. Nie, G. Liu, A. Liang, Y. Zhang, B. Shen, J. Liu, C. Hu, *et al.*, Physical Review B **94**, 241119 (2016).
[21] K. Deng, G. Wan, P. Deng, K. Zhang, S. Ding, E. Wang, M. Yan, H. Huang, H. Zhang, Z. Xu, J. Denlinger, A. Fedorov, H. Yang, W. Duan, H. Yao, Y. Wu, S. Fan, H. Zhang, X. Chen, and S. Zhou, Nature Physics **12**, 1105 (2016).
[22] L. Huang, T. M. McCormick, M. Ochi, Z. Zhao, M.-T. Suzuki, R. Arita, Y. Wu, D. Mou, H. Cao, J. Yan, N. Trivedi, and A. Kaminski, Nature Materials **15**, 1155 (2016).

[23] A. Tamai, Q. S. Wu, I. Cucchi, F. Y. Bruno, S. Ricc, T. K. Kim, M. Hoesch, C. Barreteau, E. Giannini, C. Besnard, A. A. Soluyanov, and F. Baumberger, Physical Review X **6**, 031021 (2016).

[24] J. Jiang, Z. Liu, Y. Sun, H. Yang, C. Rajamathi, Y. Qi, L. Yang, C. Chen, H. Peng, C. Hwang, *et al.*, Nature Communications **8**, 13973 (2017).

[25] I. Belopolski, D. S. Sanchez, Y. Ishida, X. Pan, P. Yu, S.-Y. Xu, G. Chang, T.-R. Chang, H. Zheng, N. Alidoust, *et al.*, Nature Communications **7**, 13643 (2016).

[26] I. Belopolski, S.-Y. Xu, Y. Ishida, X. Pan, P. Yu, D. S. Sanchez, H. Zheng, M. Neupane, N. Alidoust, G. Chang, *et al.*, Physical Review B **94**, 085127 (2016).

[27] X. Qian, J. Liu, L. Fu, and J. Li, Science **346**, 1344 (2014).

[28] K.-A. N. Duerloo, Y. Li, and E. J. Reed, Nature Communications **5**, 4214 (2014).

[29] S. Cho, S. Kim, J. H. Kim, J. Zhao, J. Seok, D. H. Keum, J. Baik, D.-H. Choe, K. Chang, K. Suenaga, *et al.*, Science **349**, 625 (2015).

[30] K.-A. N. Duerloo and E. J. Reed, ACS Nano **10**, 289 (2015).

[31] Y. Li, K.-A. N. Duerloo, K. Wauson, and E. J. Reed, Nature Communications **7**, 10671 (2016).

[32] Y. Wang, J. Xiao, H. Zhu, Y. Li, Y. Alsaid, K. Y. Fong, Y. Zhou, S. Wang, W. Shi, Y. Wang, *et al.*, Nature **550**, 487 (2017).

[33] M. Wuttig and N. Yamada, Nature Materials **6**, 824 (2007).

[34] Q. Wang, E. T. Rogers, B. Gholipour, C.-M. Wang, G. Yuan, J. Teng, and N. I. Zheludev, Nature Photonics **10**, 60 (2016).

[35] C. Zhang, S. KC, Y. Nie, C. Liang, W. G. Vandenberghe, R. C. Longo, Y. Zheng, F. Kong, S. Hong, R. M. Wallace, *et al.*, ACS nano **10**, 7370 (2016).

[36] D. Rhodes, D. Chenet, B. Janicek, C. Nyby, Y. Lin, W. Jin, D. Edelberg, E. Mannebach, N. Finney, A. Antony, *et al.*, Nano Letters **17**, 1616 (2017).

[37] Z. Dai, W. Jin, M. Grady, J. T. Sadowski, J. I. Dadap, R. M. Osgood, and K. Pohl, Surface Science **660**, 16 (2017).

[38] W. Jin, S. Vishwanath, J. Liu, L. Kong, R. Lou, Z. Dai, J. T. Sadowski, X. Liu, H.-H. Lien, A. Chaney, *et al.*, Physical Review X **7**, 041020 (2017).

[39] Z. Dai, W. Jin, J.-X. Yu, M. Grady, J. T. Sadowski, Y. D. Kim, J. Hone, J. I. Dadap, J. Zang, R. M. Osgood Jr, *et al.*, Physical Review Materials **1**, 074003 (2017).

[40] D. Rhodes, R. Schönemann, N. Aryal, Q. Zhou, Q. Zhang, E. Kampert, Y.-C. Chiu, Y. Lai, Y. Shimura, G. McCandless, *et al.*, Physical Review B **96**, 165134 (2017).

[41] G. Kresse and J. Furthmüller, Physical review B **54**, 11169 (1996).

[42] P. E. Blöchl, Physical review B **50**, 17953 (1994).

[43] J. P. Perdew, K. Burke, and M. Ernzerhof, Physical review letters **77**, 3865 (1996).

[44] A. Tkatchenko and M. Scheffler, Physical review letters **102**, 073005 (2009).

[45] D. L. Adams, Surface Science **519**, 157 (2002).

[46] J. Pendry and G. P. Alldredge, Physics Today **30**, 57 (1977).

[47] M. A. Van Hove and S. Y. Tong, *Surface crystallography by LEED: theory, computation and structural results*, Vol. 2 (Springer Science & Business Media, 2012).

[48] B. E. Brown, Acta Crystallographica **20**, 268 (1966).